IAA-AAS-DyCoSS2-14-11-02

A METHOD TO EVALUATE THE PERTURBATION OF NON-SPHERICAL BODIES

Flaviane C. F. Venditti,[*] Antonio F. B. A. Prado[†]

The purpose of this work is to show an analysis made using a method to measure the amount of perturbation in a trajectory of a spacecraft using the integral of the acceleration over the time. This integral gives the change in the velocity, meaning that the smaller the change is, the reduced will be the effect of the perturbation. The results are generated for trajectories around oblate and prolate spheroids, representing an irregular body. Because of the non-spherical shape, the trajectory around these bodies will not be like a keplerian orbit. Knowing the change of velocity, it is possible to search for the least perturbed orbits and, consequently, the more stable orbits, which can be very helpful for space missions.

INTRODUCTION

The study of perturbations is very important when there are satellites involved. The forces acting on a space vehicle must be known in order to avoid damages or changes in its orbit. For missions where the target is to study small celestial bodies closely, it is important to take into account the gravitational perturbation due to the irregularity of the body. Knowing the perturbations, it is possible to choose the orbits which have less influence on the satellite, for example. Consequently, it is expected that the orbital maneuvers required to correct the orbit of the spacecraft due to the perturbations will be smaller in magnitude and frequency, so reducing the fuel consumption. In this work a method to analyze the amount of change in the velocity is applied to irregular bodies.[1] The only perturbation considered here is the gravitational perturbation due to the non-spherical shape of the body.

The Solar System is filled with small bodies, and most of them are located between the orbits of Mars and Jupiter, in the Main Asteroid Belt. A category called NEA, or Near Earth Asteroid, is composed by celestial bodies that have trajectories passing near the orbit of the Earth.[2,3] Another important point to consider is the majority of the asteroids have irregular shapes and are rotating bodies[4, 5, 6], which makes the task of studying orbits around them more difficult. Those characteristics explain why to make some generic mapping of orbits around those bodies can be very important and useful in the mission design phase. After making a more general decision about which

[*] Postdoctoral, Orbital Mechanics and Control Division, INPE, Av dos Astronautas 1758, SJC-SP, Brazil, flaviane.venditti@gmail.com
[†] Researcher, Orbital Mechanics and Control Division, INPE, Av dos Astronautas 1758, SJC-SP, Brazil, antonio.prado@inpe.br

orbits to use, more detailed studies can be done using mathematical models that are more accurate.

PROBLEM FORMULATION

Many small bodies that are known at the present time have elongated shapes that can be approximated by ellipsoids.[7, 8] There are many forms to represent the potential of those bodies, and one of the most common solution found in the literature consider that the asteroids with ellipsoid shapes can be modeled in terms of spherical harmonics expansion.[9, 10, 11] In this paper, a closed form for the gravitational potential of the spheroids will be used, based in the results shown by Kellog[12] and MacMillan.[13]

Spheroids are figures that have two equal principal axes and a third axis that is different from the other two. The spheroids that are analyzed here are the prolate and the oblate cases, which are represented in Figure 1.

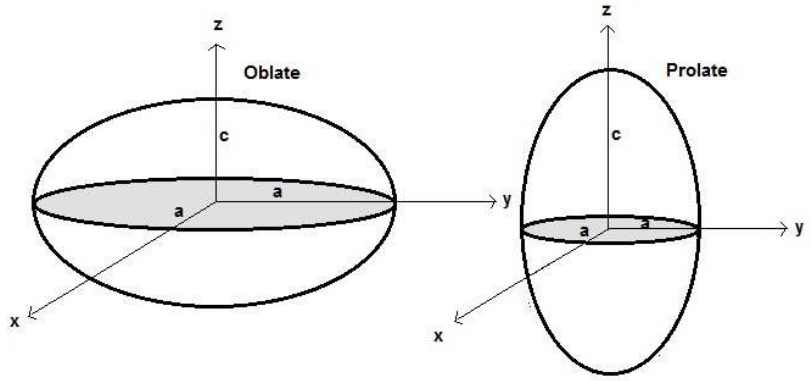

Figure 1- Oblate and prolate spheroids.

For the prolate spheroid, the major axis is *c*, and *a* are the two smaller axes. The oblate spheroid have two major axes, represented by *a*, and, in this case, a minor axis called *c*.

The non-spherical bodies considered in this work can represent well the shape of many minor bodies known in the Solar System, if the distances of the orbits of the spacecraft are not too close to the surface of the asteroid. For cases that require a more precise model, for example when a very close proximity to the asteroid is required, or even a descent trajectory to the surface of the asteroid is considered, it would be recommended to choose another model for the potential. Several choices are available in the literaure[11, 14, 15] However, the intention of the method that is presented here is to evaluate for which orbits the perturbation is larger or smaller and how fast is the change in the orbital elements due to this perturbation. Thus, the purpose is not to obtain the precise values of the disturbing forces or the fuel consumption to make station-keeping maneuvers, but to find families of less perturbed orbits, which can be good candidates to place a spacecraft, if the goal is to minimize orbital variations.

The potential of oblate and prolate spheroids are given by Equations (1) and (2), respectively.[12, 13] The difference of the two cases of spheroids is that for an oblate spheroid $a > c$, and for the prolate spheroid $c > a$.

$$V = \frac{a^2 c\sigma\sqrt{c^2+k}\pi(x^2+y^2)}{(a^2-c^2)(a^2+k)} - \frac{2a^2 c\sigma\pi z^2}{(a^2-c^2)\sqrt{c^2+k}} + \frac{2a^2 c\sigma\pi(1-\frac{x^2+y^2-2z^2}{2(a^2-c^2)})\mathrm{ArcSin}[\sqrt{\frac{a^2-c^2}{a^2+k}}]}{\sqrt{a^2-c^2}} \quad (1)$$

Where a and c are the axes, and σ the density of the body, assumed to be constant.

$$V = -\frac{a^2 c\sigma\sqrt{c^2+k}\pi(x^2+y^2)}{(-a^2+c^2)(a^2+k)} + \frac{2a^2 c\sigma\pi z^2}{(-a^2+c^2)\sqrt{c^2+k}} + \frac{2a^2 c\sigma\pi(1+\frac{x^2+y^2-2z^2}{2(-a^2+c^2)})\mathrm{ArcSinh}[\sqrt{\frac{-a^2+c^2}{a^2+k}}]}{\sqrt{-a^2+c^2}} \quad (2)$$

According to MacMillan[13], the term k in the equations for the potential of spheroids satisfies the Equation (3) shown below.

$$\frac{x^2+y^2}{a^2+k} + \frac{z^2}{c^2+k} = 1 \quad (3)$$

The density can be written as a function of the total mass of the body, and this relation is given by Equation (4).

$$\sigma = \frac{3M}{4a^2 c\pi} \quad (4)$$

In this equation M is the mass, a and c are the axes of the spheroid. The gravitational potential will then be used to obtain the perturbation integral, or *PI*, which can be seen in previous works available in the literature.[1, 16-20] This integral gives the change in the velocity caused by the perturbation, and it depends on the initial conditions of the body and the spacecraft. Therefore, by testing several different configurations for the initial orbits, it is possible to look for the cases where the trajectory is less affected. This integral is given by Equation (5). [1, 16-20]

$$PI = \int_0^T |Grad(V)|\mathrm{d}t \quad (5)$$

To be able to work with the eccentric anomaly, some arrangements needs to be made. The mean anomaly M is written in the form given by Equation (6). The derivative of M is obtained in Equation (7). After some algebraic manipulations, the resulting equation for the perturbation integral, as a function of the eccentric anomaly E, can be seen in Equation (9).[1]

$$M = M_o + n(t - t_o) = E - e\sin(E) \quad (6)$$

$$dM = ndt = (1 - ecos(E))dE \quad (7)$$

$$dt = \frac{(1-ecos(E))dE}{n} \quad (8)$$

$$PI = \frac{1}{n}\int_0^{2\pi} |\text{Grad(V)}|(1 - ecos(E))dE \tag{9}$$

In those equations *n* is the mean motion, *e* the eccentricity, *Grad (V)* is the gradient of the potential, and *E* is the eccentric anomaly.

To calculate the perturbation integral, the partial derivatives are obtained from Equations (1) and (2). The *PI* considers only the disturbing term, so the keplerian term is subtracted from the equations for the potential before the gradient is calculated. Equations (10), (11) and (12) show, for the oblate spheroid case, the derivatives with respect to *x*, *y*, and *z*, respectively.

$$\frac{\partial V}{\partial x} = \frac{1}{2}GMx\left[\frac{3\sqrt{c^2+k}}{(a^2-c^2)(a^2+k)} + \frac{2}{(x^2+y^2+z^2)^{3/2}} - \frac{3\text{ArcSin}\left(\sqrt{\frac{a^2-c^2}{a^2+k}}\right)}{(a^2-c^2)^{3/2}}\right] \tag{10}$$

$$\frac{\partial V}{\partial y} = \frac{1}{2}GMy\left[\frac{3\sqrt{c^2+k}}{(a^2-c^2)(a^2+k)} + \frac{2}{(x^2+y^2+z^2)^{3/2}} - \frac{3\text{ArcSin}\left(\sqrt{\frac{a^2-c^2}{a^2+k}}\right)}{(a^2-c^2)^{3/2}}\right] \tag{11}$$

$$\frac{\partial V}{\partial z} = GMz\left[\frac{3}{(-a^2+c^2)\sqrt{c^2+k}} + \frac{1}{(x^2+y^2+z^2)^{3/2}} + \frac{3\text{ArcSin}\left(\sqrt{\frac{a^2-c^2}{a^2+k}}\right)}{(a^2-c^2)^{3/2}}\right] \tag{12}$$

Where *G* is the gravitational constant with value of 6.6738×10^{-11} $m^3/kg.s^2$. The same process of obtaining the partial derivatives is made for the case of a prolate spheroid. The results are shown in Equations (13) to (15).

$$\frac{\partial V}{\partial x} = \frac{1}{2}GMx\left[\frac{3\sqrt{c^2+k}}{(a^2-c^2)(a^2+k)} + \frac{2}{(x^2+y^2+z^2)^{3/2}} + \frac{3\text{ArcSinh}\left(\sqrt{\frac{-a^2+c^2}{a^2+k}}\right)}{(-a^2+c^2)^{3/2}}\right] \tag{13}$$

$$\frac{\partial V}{\partial y} = \frac{1}{2}GMy\left[\frac{3\sqrt{c^2+k}}{(a^2-c^2)(a^2+k)} + \frac{2}{(x^2+y^2+z^2)^{3/2}} + \frac{3\text{ArcSinh}\left(\sqrt{\frac{-a^2+c^2}{a^2+k}}\right)}{(-a^2+c^2)^{3/2}}\right] \tag{14}$$

$$\frac{\partial V}{\partial z} = GMz\left[\frac{3}{(-a^2+c^2)\sqrt{c^2+k}} + \frac{1}{(x^2+y^2+z^2)^{3/2}} - \frac{3\text{ArcSinh}\left(\sqrt{\frac{-a^2+c^2}{a^2+k}}\right)}{(-a^2+c^2)^{3/2}}\right] \tag{15}$$

In order to normalize the results, the integral of the partial derivatives, that gives the *PI,* is divided by 2π.

RESULTS

Oblate Spheroid

The amount of perturbation over time may now be analyzed calculating the integral of the potential derivatives over a period of time. Several initial configurations can be used to test which one have the minimum value for the perturbation integral. First the results for the case of an oblate spheroid are shown. The initial values used in the following results are: the dimensions of the oblate spheroid is 5 km for the major axes and 2.5 km for the minor axis; the orbital radius for the oblate and prolate cases is 10 km; the mass considered, also for both cases, is $2x10^{13}$ kg. Figure 2 shows the acceleration as a function of the inclination of the orbit for one orbital period, considering a circular orbit.

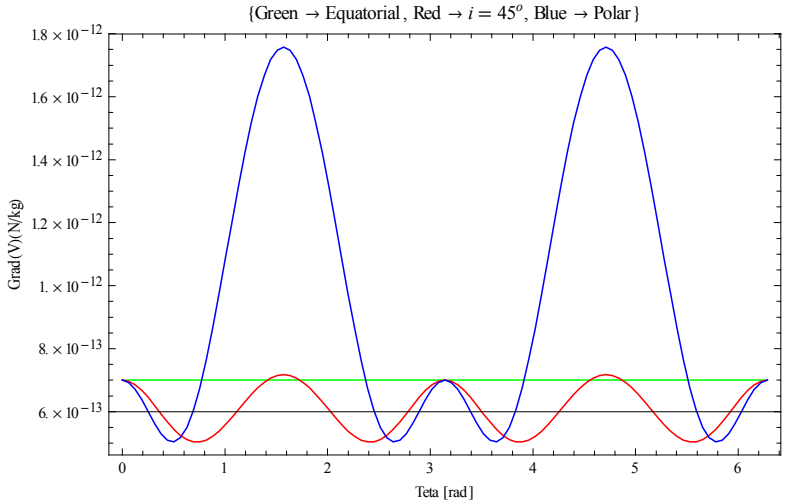

Figure 2- Acceleration for one revolution for an oblate spheroid.

The oblate spheroid has two equal major axes, thus the acceleration for an equatorial orbit is constant in every point of the orbit. Figure 2 shows that the variation of the acceleration is much higher for polar orbits. That is because the *c* axis measures half of the length of the major axes, so when it passes closer to the body, the acceleration grows, and decreases after leaving these nearest locations. Therefore, the inclination of 90^o is the situation in which the acceleration varies the most. This result is expected, in general, but the results shown here uses a new way to quantify those differences observed.

Using Equation (9), Figure 3 shows the evolution of the perturbation integral, as a function of the inclination for one orbital period, also considering a circular orbit. Figure 3 shows that the maximum variation of the *PI* happens when the inclination is 90^o, which is a polar orbit, and it is where the size of axis suffers more changes during the revolution, confirming what was explained

for the acceleration. Besides that maximum, it is also noted a minimum value, near the inclination of 0.6 radians, equivalent to 34 degrees. Next, the perturbation integral is shown again, now as a function of the inclination, but for elliptic orbits, with several values for the eccentricity.

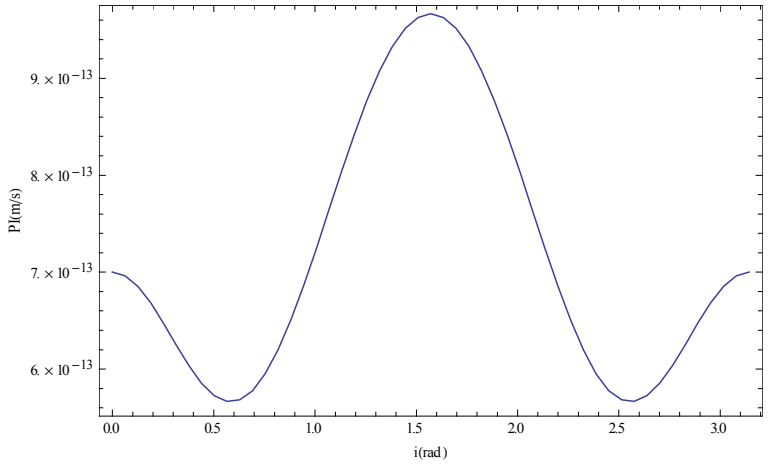

Figure 3- Perturbation integral as a function of the inclination for an oblate spheroid in a circular orbit.

From Figure 4, that shows five values of eccentricities, from zero to 0.4, it can be seen that, the more eccentric is the orbit, the lager will the change in the velocity due to the perturbation, which means that the orbit is more perturbed. When the orbit starts being more elliptic, the equatorial orbit begins to have higher values for the *PI*, due to the fact that the oblate spheroid has the major axes in the equatorial plane. Therefore, as the eccentricity increases, the periapsis of the orbit becomes increasingly close to the body, resulting on a higher perturbation in these points.

The distance from the body is also a point to be analyzed. The orbital radius considered up to this point is 10 km. The results for the perturbation integral for a semi-major axis from 10 km to 25 km can be seen in Figure 5, for inclinations of 0, 45^{o}, and 90^{o} , always considering a circular orbit.

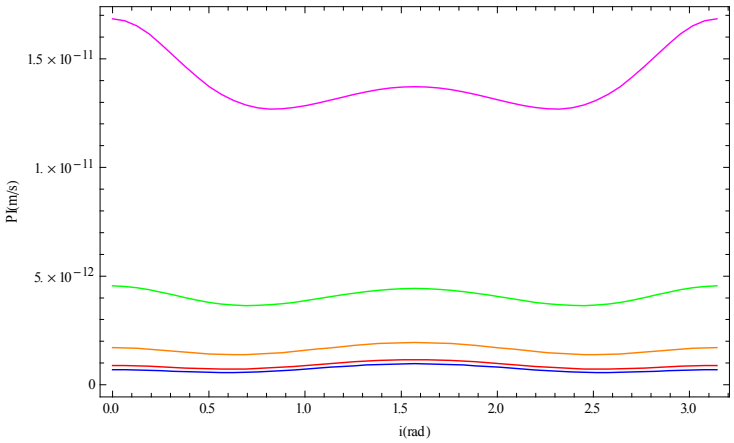

Figure 4- Perturbation integral versus inclination for an oblate spheroid. Blue, e = 0; Red, e = 0.1; Orange, e = 0.2; Green, e = 0.3; Magenta, e = 0.4.

The same initial data used in the previous graphic is shown in Figure 6, but also for the case of elliptic orbits. The values for the eccentricity used were: zero, 0.1, 0.2, 0.3 and 0.4.

The effect of different values for the eccentricity can now be seen alone, in Figure 7, for an orbit with semi-major axis of 10 km.

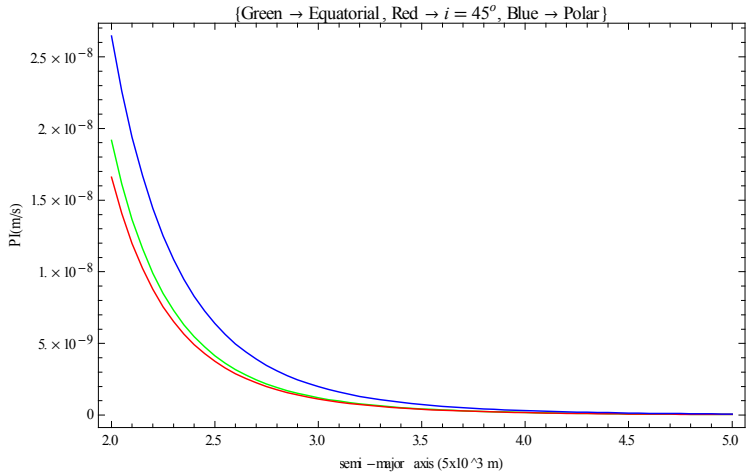

Figure 5- Perturbation integral versus semi-major axis for circular orbit, for oblate spheroid.

The eccentricity has about the same affects for orbits with inclinations of 0, 45°, and 90°, changing slightly faster for the equatorial orbits because of the major axes. Because the major axis is twice the size of the minor axis, as the eccentricity increases, it may reach the situation of colliding with the body at the periapsis first for the equatorial plane, as explained before. In all cases, the perturbation integral grows very fast between the values of 0.4 and 0.5 for the eccentricity, because of the proximity from the body. The increase of the perturbation when getting closer to the body was discussed in the previous results, and is confirmed in Figure 7.

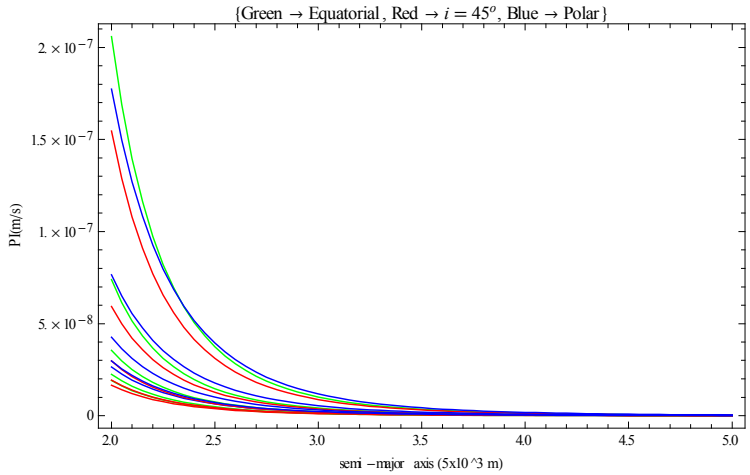

Figure 6- Perturbation integral versus semi-major axis for eccentricity from 0 to 0.4. Green is equatorial orbit; Red is for $i = 45^o$; Blue is polar orbit.

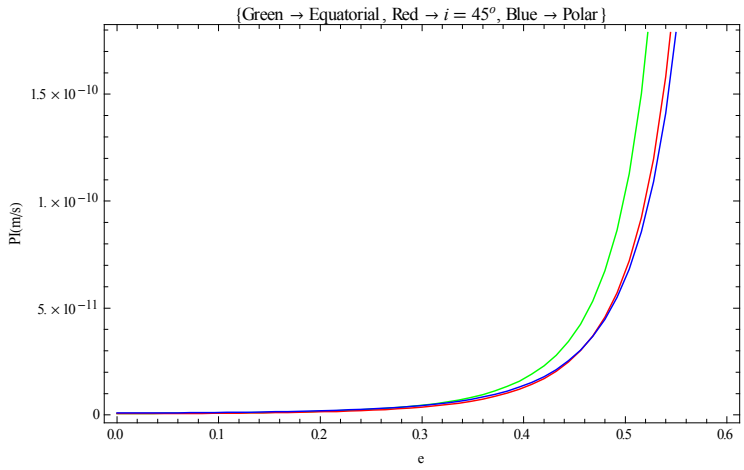

Figure 7- Perturbation as a function of eccentricity for $i = 0$,$i = 45^o$, and $i = 90^o$.

Another test that will be presented next is to vary the value of the major axis *a*. Figure 8 shows the *PI* as a function of the major axis with values ranging from 3 km to 7 km.

When the value for the *a* axis is larger, it differs more from the *c* axis, which measures 2.5 km. In other words, for the chosen parameters, it is when the body is more elongated. For the lowest value of *a*, which is 3 km, the difference from the *c* axis is smaller, getting close to become a sphere. In the case of a homogeneous sphere, the *PI* should suffer no changes for a circular orbit for any inclination, because the gravitational force is the same everywhere around it.

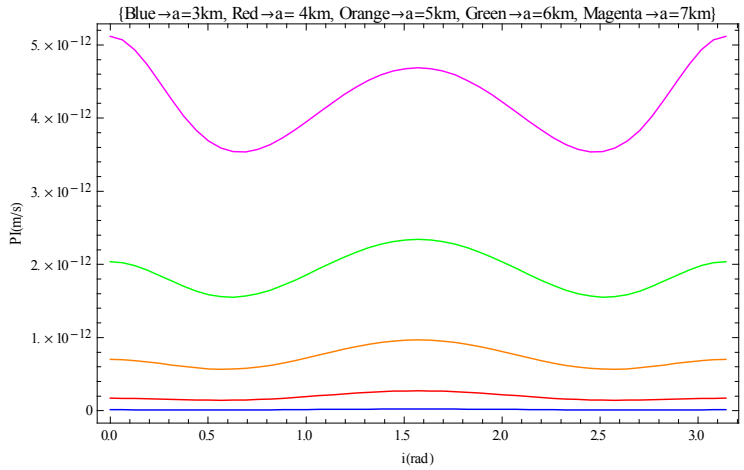

Figure8- Perturbation integral as a function of the inclination for different values for *a* axis.

Prolate Spheroid

Some results will also be presented now for the prolate spheroid. The same values used in the previous results for the mass and orbital radius are used here. The minor axis *a* is considered to

measure 2.5 km, and the major axis *c* is 5 km. The acceleration for one revolution is shown in Figure 9 for the prolate spheroid with inclinations of 0°, 45°, and 90°, considering a circular orbit.

Since the two minor axes in the equatorial plane are the same, it is possible to see in Figure 9 that the acceleration is constant. For an inclination of 45° a small variation starts to appear. It is very noticeable that, for polar orbits, the acceleration varies the most. This is because the major axis *c* is twice the length of the minor axes, and for an inclination of 90° the orbit passes by the two extreme values.

Figure 10 shows the perturbation integral as a function of the inclination for the following values of eccentricity: 0, 0.1, 0.2, 0.3, 0.4, and 0.5. As for the oblate spheroid, in equatorial orbits there is no change in the size of the axes, because both axes have equal measurements. Therefore, the change in the velocity is greater for polar orbits. Because the major axis for the prolate spheroid is the *c* axis, which is in the polar plane, even with the increase of the eccentricity, the polar orbits are still the most perturbed cases, different from the oblate spheroid.

The change in the velocity is greater for very eccentric orbits, and because of the elongated shape of the prolate spheroid, the pattern of the *PI* being higher for polar orbits is the same, just changing the magnitude.

The variation of the orbital radius is studied ranging from 10 km to 25 km, and the *PI* is presented as a function of the semi-major axis for a circular orbit in Figure 11. For closer orbits, it is noticed that, for an inclination of 90°, the perturbation integral shows higher values. For inclinations of zero and 45° the results are practically the same. When the semi-major axis of the orbit increases, which means that it is moving away from the body, the *PI* decreases. This is consistent with the fact that, the closer from an irregular body, the greater will be the effects of the perturbation on an object around it.

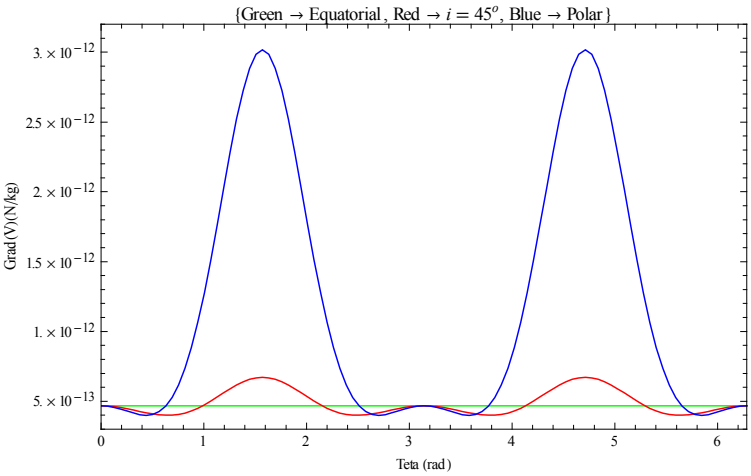

Figure 9- Acceleration for one revolution for a prolate spheroid.

The next result, in Figure 12, shows the perturbation integral as a function of the eccentricity. The green and red lines, representing the cases for i= 0 and i= 45°, respectively, arealmost superimposed, as it was for the variation in the semi-major axis. The rise of the change in velocity happens faster when the orbit starts getting more eccentric. After eccentricity of 0.4, the *PI* grows rapidly, even faster for polar orbits, because it is getting too close to the body.

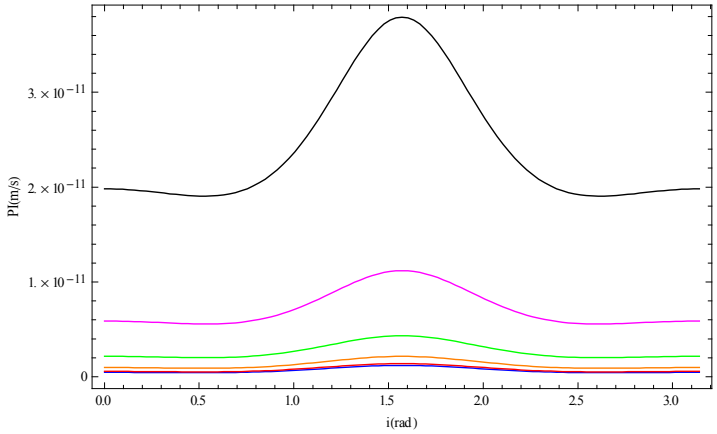

Figure 10- Perturbation integral versus inclination for a prolate spheroid. Blue, e= 0; Red, e=0.1; Orange, e=0.2; Green, e= 0.3; Magenta, e= 0.4; Black, e= 0.5.

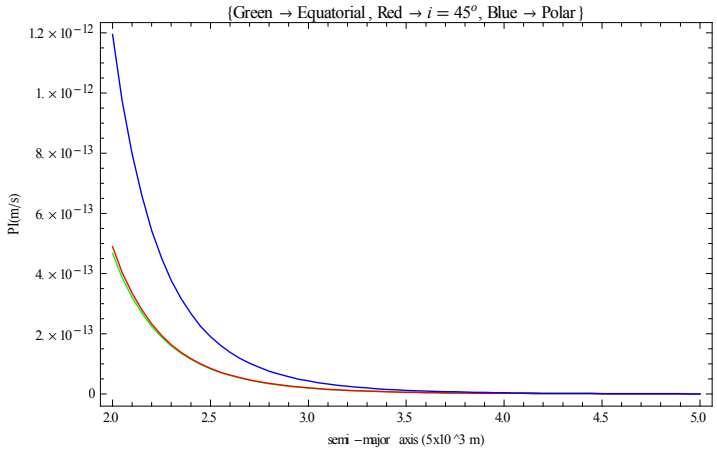

Figure 11- Perturbation integral versus semi-major axis for circular orbit for a prolate spheroid.

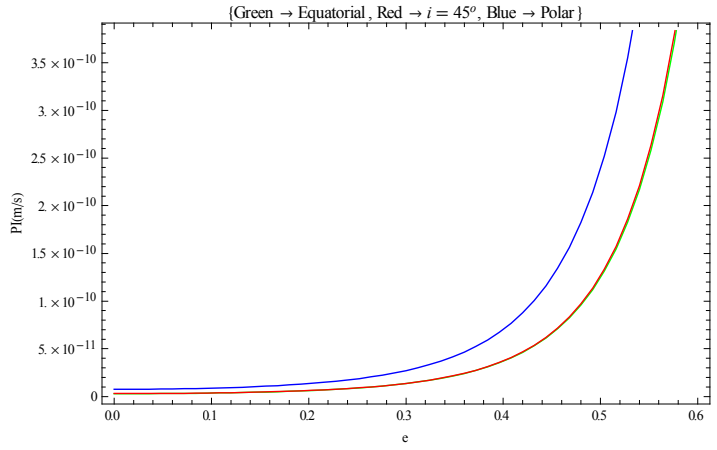

Figure 12- Perturbation as a function of eccentricity for i= 0, i= 45^o, and i= 90^o, with a=10km.

Figure 13considers the variation of the *a* axis, which for the prolate spheroid is the minor axis. The values for *a* goes from 500m to 4 km. Recalling that, the *c* axis used here measures 5 km.

For smaller values for the minor axis the *PI* has higher values, because the body is more like an ellipsoid. When the value for the minor and major axes are almost the same, represented in magenta color in the figure above, the perturbation is minor, because the shape of the object is approximately like a sphere, as was already explained for the oblate spheroid previously.

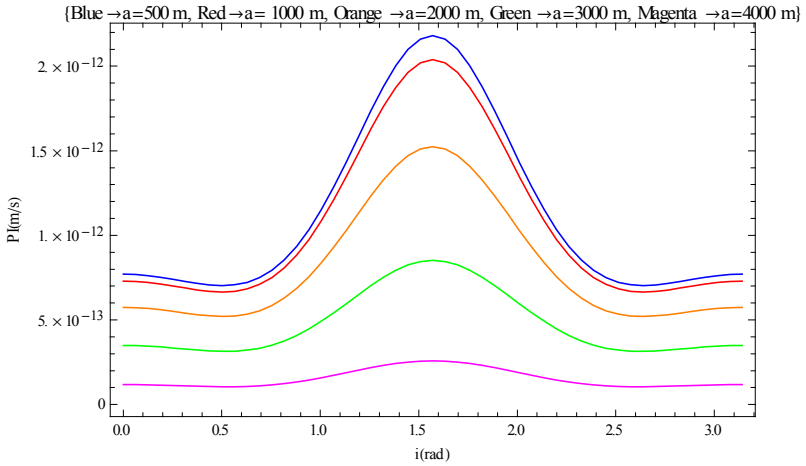

Figure 13- Perturbation integral as a function of the inclination for a prolate spheroid for different values for *a*axis.

Rotation

The results already presented considered an orbit around a fixed body. Using ellipsoids to represent small celestial bodies is a valid approximation in most cases, but it is important to remember that asteroids are spinning and some of them quite fast. The rotation of small bodies can be deduced, for example, from light curves.[5,23, 24] Most of the asteroids are rotating around its principal axis, which is the one of the largest moment of inertia. Very few are in a different types of rotation, like asteroid Toutatis, that is in a complicated tumbling rotation.[25, 26] Therefore, the results presented here will consider that the spacecraft is in a circular orbit around a rotating celestial body. For the oblate spheroid case, results with rotation in the three axis were obtained. Figure 14 considers rotation in the *z* axis for several rotational periods, denoted by R (R = 0 means no rotation).

Because of the symmetry of having two equal axes, the rotation for a spheroid in the *z* axis is not affected by the change in the angular velocity. This is true for both spheroids, oblate and prolate. Changing the axis of rotation generates different results. Figure 15 and 16, consider rotation in the *y* and *x* axis, respectively, and show the perturbation integral as a function of the inclination.

In Figures 15 and 16, as the rotation period changes, the difference of the behavior of the curves can be noticed. For the *x* and *y* axes, the case with no rotation, in blue line, and the case of the slowest rotation, in magenta, are very similar. As for the other values of angular velocity, the *PI* varies differently for each particular case. It is clear that the rotation of the celestial body may

increase or decrease the total perturbation. In the example shown in Figure 15 the rotation with a period of 48 hours has the minimum average perturbation. The relative differences are not negligible, which means that the rotation must be taken into account to get accurate results. It is also noted that the minimums are not only different in terms of magnitude, but their locations are also modified. It means that the solution of the problem of finding the less perturbed orbits depends on the speed of rotation. Therefore, it is important to know this information in order to make a better orbit selection.

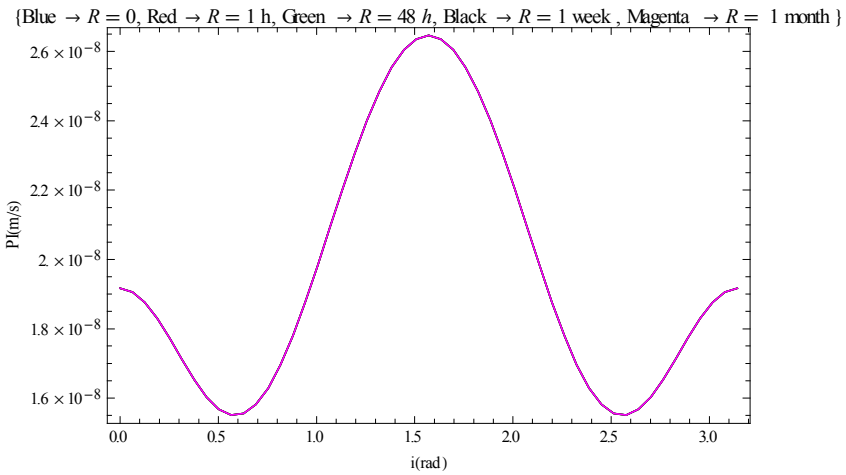

Figure 14- Perturbation integral versus inclination for different rotation periods in z axis for an oblate spheroid.

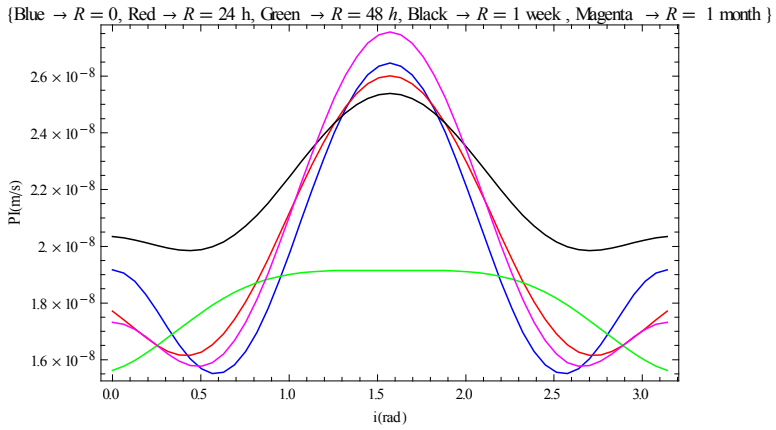

Figure 15- Perturbation integral versus inclination for different rotation periods around the y axis.

The examples shown above considered a prograde rotation. Considerations for retrograde rotation can also be made. For rotation in any of the axis, the polar orbit tends to have much higher values for the *PI*, which is expected, since the different axis is in the polar plane.

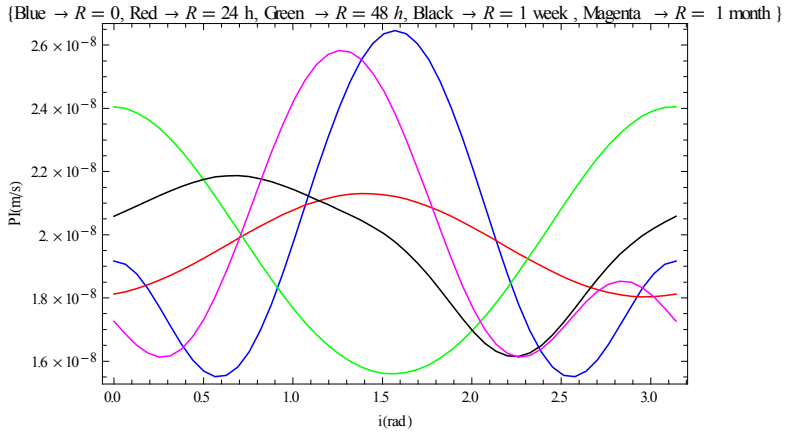

Figure 16- Perturbation integral versus inclination for different rotation periods around the x axis.

Lagrange's Planetary Equations

For bodies that are not point masses, the variations of each orbital element can be obtained using the planetary equations of Lagrange. This set of six differential equations gives the rates of change of the elements considering the disturbing function.[22] Equations 16 to 21 are the six equations.

$$\frac{da}{dt} = \frac{2}{na}\frac{\partial V}{\partial M} \tag{16}$$

$$\frac{de}{dt} = \frac{1-e^2}{na^2 e}\frac{\partial V}{\partial M} - \frac{\sqrt{1-e^2}}{na^2 e}\frac{\partial V}{\partial \omega} \tag{17}$$

$$\frac{di}{dt} = -\frac{1}{na^2\sqrt{1-e^2}\sin i}\frac{\partial V}{\partial o} + \frac{\cos i}{na^2\sqrt{1-e^2}\sin i}\frac{\partial V}{\partial \omega} \tag{18}$$

$$\frac{d\omega}{dt} = \frac{\sqrt{1-e^2}}{na^2 e}\frac{\partial V}{\partial e} - \frac{\cos i}{na^2\sqrt{1-e^2}\sin i}\frac{\partial V}{\partial i} \tag{19}$$

$$\frac{do}{dt} = \frac{1}{na^2\sqrt{1-e^2}\sin i}\frac{\partial V}{\partial i} \tag{20}$$

$$\frac{dM}{dt} = n - \frac{2}{na}\frac{\partial V}{\partial a} - \frac{1-e^2}{na^2 e}\frac{\partial V}{\partial e} \tag{21}$$

Figures 16 to 24 show the results of the rate of variation of the orbital elements, as predicted by the Lagrange planetary equations. Those plots are also an alternative to make mappings that identifies orbits that are less perturbed, therefore complementing the integral approach in helping to find orbits that are more stable, by having smaller initial variations rate at the beginning of the

orbit. It is clear that there is a good correlation between the curves generated by the integral approach and the variation of the elements. An exact correspondence is not expected, because the integral approach measure the total perturbation received by the satellite, which perturbs all the keplerian elements, while the view based in the Lagrange planetary equations shows the effects of the perturbation in each individual orbital element. So, even if a specific orbital element has a constant evolution for a situation where the integral approach shows the existence of perturbations, it is possible that there is another orbital element being disturbed.

Figures 16 to 18 show the variation of the semi-major axis as a function of the three orbital elements: semi-major axis, eccentricity and inclination, respectively. The correlation of the graphics with respect to the results obtained for the perturbation integral is very clear, showing that the contribution of this element to the perturbation is higher for smaller values for the semi-major axis. Regarding the effects of the eccentricity, shown in Figure 17, the results confirm that its increase causes more perturbation to the spacecraft. The dependence with the inclination is shown in Figure 18, that also evidence the maximum of the perturbation occurs for the polar orbit.

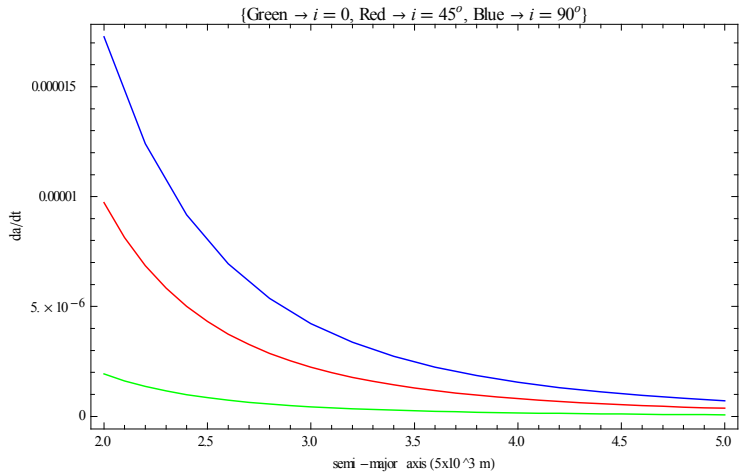

Figure 16- da/dt as a function of the semi-major axis for an oblate spheroid.

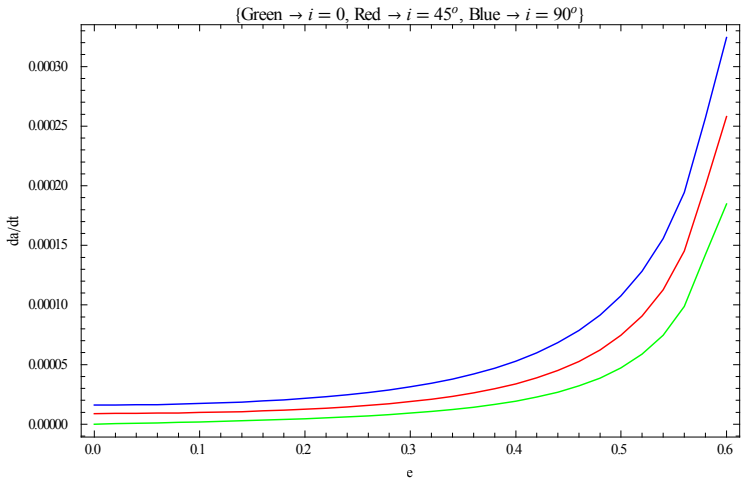

Figure 17- da/dt as a function of the eccentricity for an oblate spheroid.

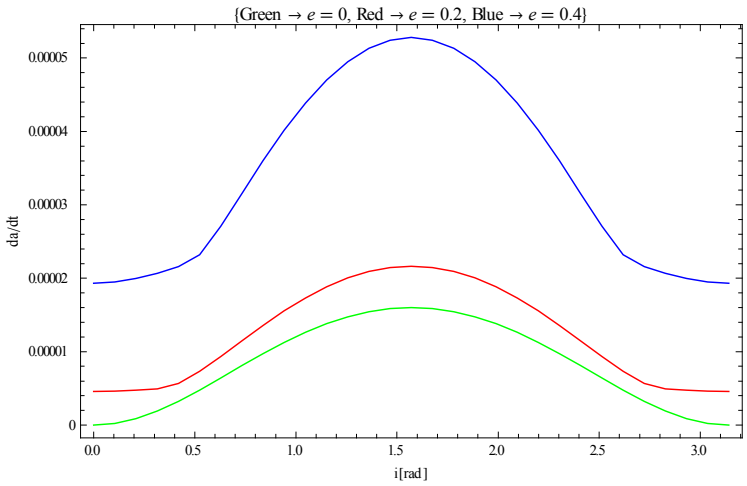

Figure 18- da/dt as a function of the inclination for an oblate spheroid, for different eccentricity values.

Next, using Equation (17), the rate of variation of the eccentricity is presented in Figures 19-21. For all the graphics there are three lines, representing different values of inclination, in which green is for equatorial orbits, red for inclination of 45°, and blue for polar orbits. Similar results are obtained for the behavior of the eccentricity as a function of the semi-major axis of the orbit (its increase reduces the effects of the perturbation) and the inclination (the peak at the polar orbits). On the opposite side, the effects of the eccentricity has a different behavior. At the beginning (small eccentricities), the increase of the eccentricity decreases the rate of variation of the eccentricity, which means that it reduces the perturbations in this orbital elements. This is opposite to the predictions made by the integral approach and the explanation for that fact is that the perturbation is acting on the other orbital elements.

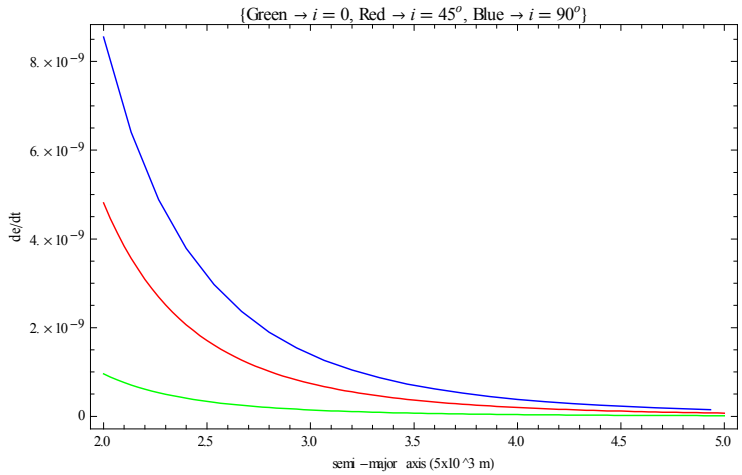

Figure 19- de/dt as a function of the semi-major axis for an oblate spheroid.

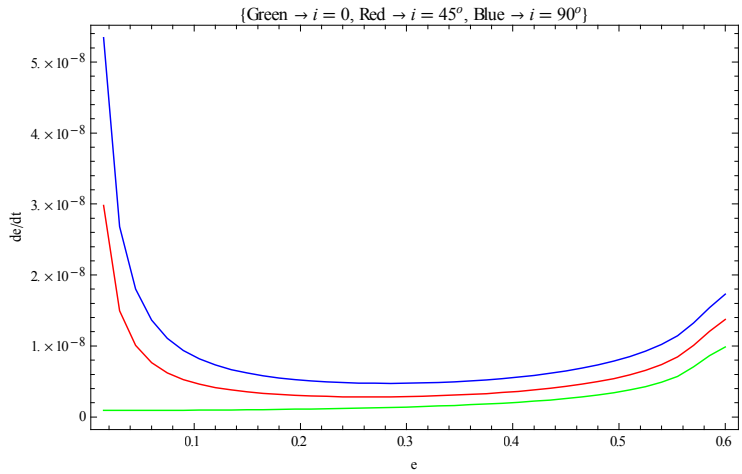

Figure 20- de/dt as a function of the eccentricity for an oblate spheroid.

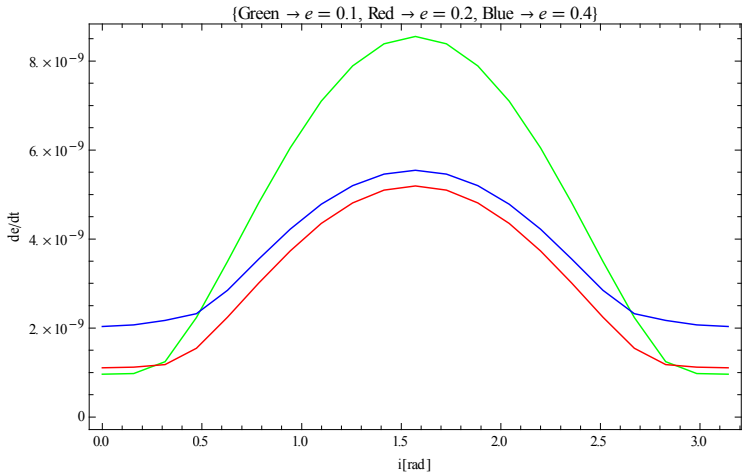

Figure 21- de/dt as a function of the inclination for an oblate spheroid, for different eccentricity values.

The following series of graphics that are shown next are made for the evolution of the rate of variation of the inclination, obtained from Equation (18). Figures 22 to 24 show the variation of the inclination as a function of the semi-major axis, the eccentricity, and the inclination, respectively. Those results are well connected with the integral approach, showing that decreasing the semi-major axis and increasing the eccentricity of the orbit increases the perturbation made in the inclination. The maximum for the polar orbits are also confirmed.

Thus, the results obtained using the Lagrange's planetary equations makes it possible to analyze the effect of each orbital element independently, and therefore, evaluate which element is more affected due to the configuration of the orbit and the celestial body shape.

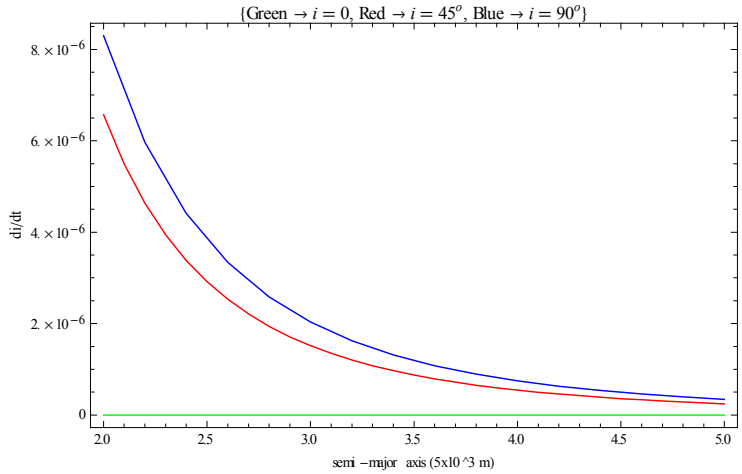

Figure 22- di/dt as a function of the semi-major axis for an oblate spheroid.

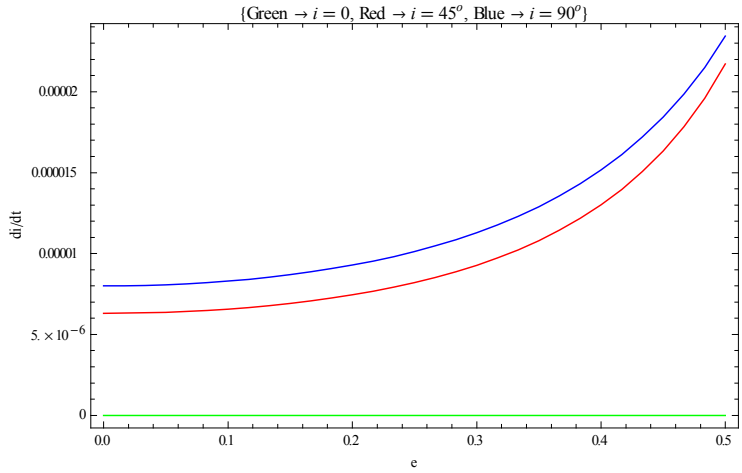

Figure 23- di/dt as a function of the eccentricity for an oblate spheroid, for different inclinations.

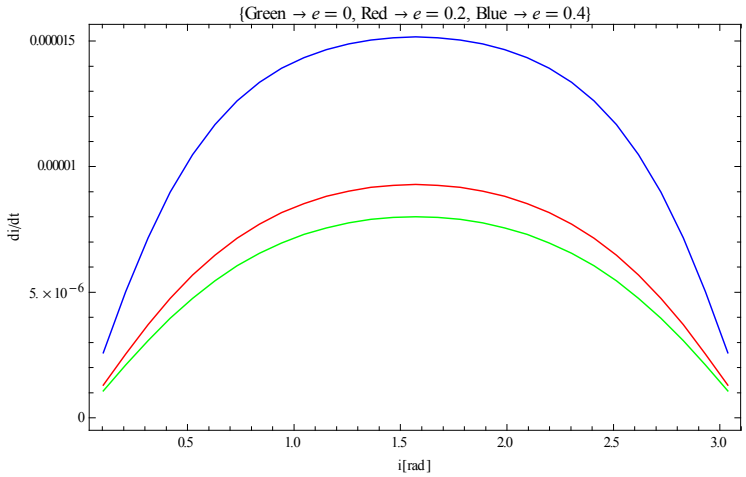

Figure 24- di/dt as a function of the inclination for an oblate spheroid, for different eccentricities.

In order to complement the results generated so far, the gravitational acceleration was used to plot trajectories to finalize the analyses. Figure 25 shows, for the oblate spheroid, 200 revolutions for an equatorial orbit, where: image *a* considers a circular orbit and semi-major axis of 10 km; image *b* is made for an elliptic orbit (e = 0.3) with the same value for the semi-major axis. It is clear the effects of the larger perturbation in the eccentric orbit. Remember that the dimensions of the oblate spheroid are 5 km and 2.5 km for the major and minor axis, respectively, and the mass is $2x10^{13}$ kg.

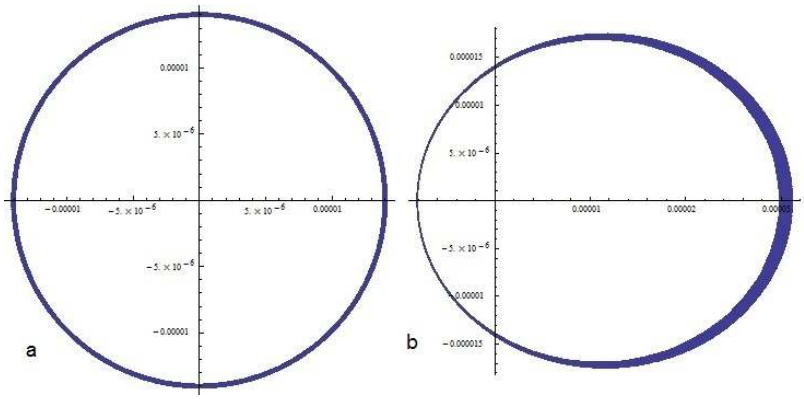

Figure 25 - Oblate spheroid, i = 0, 200 revolutions, semi-major axis = 10 km. a) e = 0; b) e = 0.3.

Hereafter, on Figure 26, the configurations are the same as the previous images, except for the inclination, that in this case is 90^o. Also, there is image *c,* showing the case of a more distant orbit, with semi-major axis of 40 km. It is clear that the effect of the eccentricity is to increase the perturbation, as well as the fact that the polar orbit is more perturbed. The fact that the non-spherical shape perturbs more the orbit when closer to the body is also noticed, proving the results obtained before.

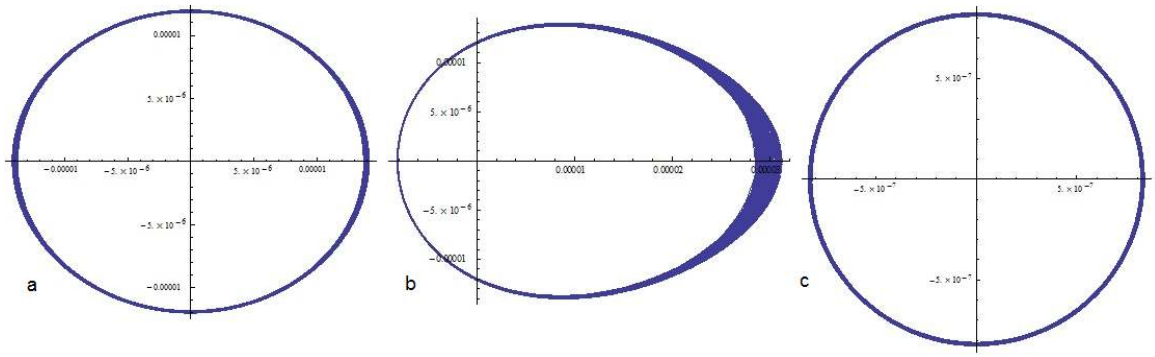

Figure 26 - Oblate spheroid, i = 90^o, 200 revolutions. a) e = 0, semi-major axis = 10 km; b) e = 0.3, semi-major axis = 10 km; c) e = 0, semi-major axis = 40 km.

The last images represented a body in a fixed position. Figures 27 and 28 consider that the body is rotating, in a circular orbit, with a period of 4 hours, for an equatorial and polar orbit, respectively. In this case it was performed five revolutions around the body. Images *a* consider rotation in the *x* axis, images *b* in the *y* axis, and on images *c* the rotation is in the *z* axis.

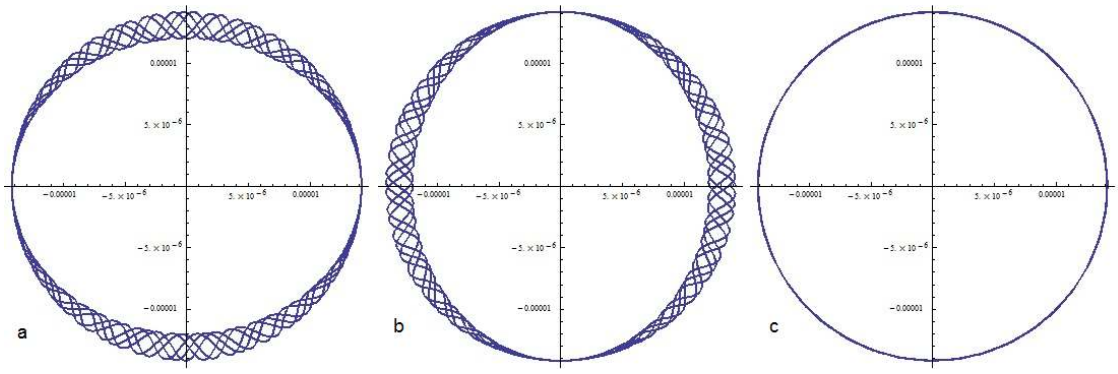

Figure 27 - Oblate spheroid, e = 0, i = 0, 5 revolutions. a) Rotation in *x* axis; b) rotation in *y* axis; c) rotation in *z* axis.

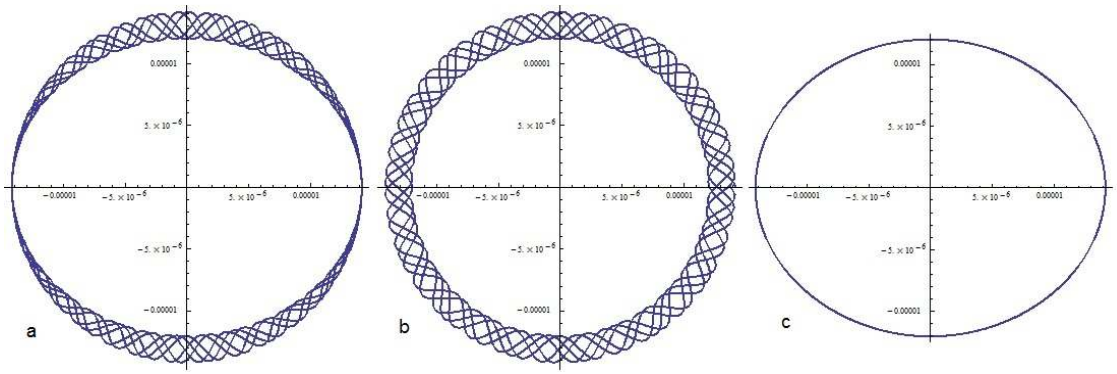

Figure 28 - Oblate spheroid, e = 0, i = 90°, 5 revolutions. a) Rotation in *x* axis; b) rotation in *y* axis; c) rotation in *z* axis.

These figures illustrate the good correlations between the integral approach, the variations based in the Lagrange´s Planetary equations and the trajectories. They confirm the configurations where the perturbation is larger, obtained with the analyses of the perturbation integral. They also show the importance of considering the right rotation axis of the object, since the intention is to make an analogy to minor bodies of the Solar System, that are rotating irregular shaped bodies.

CONCLUSION

In this work the study of perturbation of non-spherical bodies is presented. A method for evaluating the amount of perturbation depending on the initial configuration was tested. The formulation of the partial derivatives of the potential of spheroids was obtained using the equations of the potential for the specific cases that were chosen. Some results have been shown for the case of

oblate and prolate spheroids. Many cases can be tested changing the initial configurations, and then, the analyses of the cases where the perturbation is smaller can be obtained. Satellites suffer perturbations, changing their initial position, which can be controlled with the use of thrusters. Therefore, knowing the orbits that will have less effect on the satellites is a very import topic for space mission. An alternative mapping based on the Lagrange Planetary equations were made and showed a good correlation with the integral approach. The gravitational acceleration plotted also confirmed the results obtained from the other analyses. The combination of the results quantified how the increase of the semi-major axis and the decrease of the eccentricity decrease the perturbation from the irregular shape of the celestial body. It is also shown that the effects of the inclination is to generate a maximum level of perturbation for polar orbits. In this way, the present paper can help mission analyses to choose orbits that are less perturbed to place their satellites.

ACKNOWLEDGMENTS

The authors wish to express their appreciation for the support provided by grants #473387/2012-3, 473164/2013-2 and 304700/2009-6 from the National Council for Scientific and Technological Development (CNPq); grants # 2011/08171-3, 2011/13101-4, 2014/06688-7 and 2012/21023-6 from São Paulo Research Foundation (FAPESP) and the financial support from the National Council for the Improvement of Higher Education (CAPES).

REFERENCES

[1]Prado, A. F. B. A; Searching for orbits with minimum fuel consumption for station-keeping maneuvers: an application to lunisolar perturbations, Mathematical Problems in Engineering, 2013.

[2]Scheeres, D. J. Orbital Motion in Strongly Perturbed Environments. Orbital Motion in Strongly Perturbed Environments, by Scheeres, Daniel J. ISBN: 978-3-642-03255-4. Berlin: Springer, 2012.

[3]Bottke, W. F. (Ed.).. Asteroids III. University of Arizona Press, 2002.

[4]Busch, M. W. Shapes and spins of near-earth asteroids. Universal-Publishers, 2010.

[5]Pravec, P. E. T. R., Harris, A. W., & Michalowski, T. Asteroid rotations. Asteroids III, 113, 2002.

[6]Hudson, R. S., Ostro, S. J. Shape and non-principal axis spin state of asteroid 4179 Toutatis. SCIENCE-NEW YORK THEN WASHINGTON-, 84-84, 1995.

[7]Scheeres, D.J. Dynamics about uniformly rotating triaxial ellipsoids: application to asteroids. Icarus, 121, 67–87, 1994.

[8]Bartczak, P.; Breiter, S.; Jusiel, P. Ellipsoids, material points and material segments. Celestial Mechanics and Dynamical Astronomy, 2006.

[9]Scheeres, D.J., Hu,W. Secular motion in a 2nd degree and order gravity field with no rotation. Celest Celestial Mechanics and Dynamical Astronomy. 79, 183–200, 2001.

[10]Kaula, W. M. Theory of satellite geodesy. Waltham, MA: Blaisdell, 1966.

[11]Rossi, A.; Marzari, F.; Farinella, P. Orbital evolution around irregular bodies. Earth Planets and Space, v. 51, n. 11, p. 1173-1180, 1999.

[12]Kellog, O. D.; Foundations of potential theory, Dover Publications.com, 1929.

[13]MacMillan, W. D.; The theory of potential, Dover, 1930.

[14]Werner, R. A. The gravitational potential of a homogeneous polyhedron or don't cut corners. Celestial Mechanics and Dynamical Astronomy, v. 59, n. 3, p. 253-278, 1994.

[15]Geissler, P.; Petit, J.-M.; Durda, D.; Greenberg, R.; Bottke, W.; Nolan, M.; Moore, J. Erosion and eject a reaccretion on 243 Ida and its moon. Icarus, v.120, n. 1, p.140-157, 1997.

[16]Prado, A. F. B.A. Mapping Orbits Around the Asteroid $2001SN_{263}$. Advances in Space Research, v. 53, p. 877-889, 2014.

[17]Oliveira, T. C., Prado, A.F.B.A., Mapping orbits with low station keeping costs for constellations of satellites based on the integral over the time of the perturbing forces. Acta Astronautica, v.104, p. 350-361, 2014.

[18]Sanchez, D. M., Prado, A.F.B.A., Yokoyama, T. On the Effects of Each Term of the Geopotential Perturbation Along the Time I: Quasi-circular Orbits. Advances in Space Research, v.54, p.1008 - 1018, 2014.

[19]Carvalho, J. P. S., Vilhena de Moraes, R., Prado, A. F. B. A., Searching Less Perturbed Circular Orbits for a Space-craft Travelling around Europa. Mathematical Problems in Engineering (Print), 2014.

[20]Venditti, F., Prado, A. F. B. A., Mapping Orbits Regarding Perturbations due to the Gravitational Field of a Cube Mathematical Problems in Engineering, 2014.

[21]Roy, A. E. Orbital motion.CRC Press, 2004.

[22]Torppa, J. Lightcurve inversion for asteroid spins and shapes, 2007.

[23]Kaasalainen, M., Mottola, S., Fulchignoni, M., 2002. Asteroid models from disk-integrated data.In: Bottke, W.F., Cellino, A., Paolicchi, P., Binzel, R.P., (Eds.), Asteroids III, Univ. of Arizona Press, Tucson, pp. 139-150, 2002.

[24]Scheeres, D. J.; Schweickart, R. L.; The mechanics of moving asteroids. In 2004 Planetary Defense Conference: Protecting Earth from Asteroids (pp. 23-26). February, 2004.

[25]Hudson, R. S., &Ostro, S. J. Shape and non-principal axis spin state of asteroid 4179 Toutatis. SCIENCE-NEW YORK THEN WASHINGTON-, 84-84, 1995.